Published in final edited form as:
Pancreas. 2015 January ; 44(1): 64–75. doi:10.1097/MPA.0000000000000238.

Longitudinal Bioluminescence Imaging of Primary versus Abdominal Metastatic Tumor Growth in Orthotopic Pancreatic Tumor Models in NSG Mice

Harlan E. Shannon, Ph.D.[*], **Melissa L. Fishel, Ph.D.**[*,§,‡], **Jingwu Xie, Ph.D.**[*,§,‡,†], **Dongsheng Gu, M.D.**[*], **Brian P. McCarthy, B.A.**[⊥], **Amanda A. Riley, B.A.**[⊥], **Anthony L. Sinn, B.S.**[||], **Jayne M. Silver, B.S.**[||], **Kacie Peterman, H.S.D.**[||], **Mark R. Kelley, Ph.D.**[*,§,‡,†], **Helmut Hanenberg, M.D.**[*], **Murray Korc, M.D.**[§,†,¶], **Karen E. Pollok, Ph.D.**[*,§,‡,†,||], and **Paul R. Territo, Ph.D.**[⊥]

[*]Department of Pediatrics, Section of Pediatric Hematology/Oncology, Herman B Wells Center for Pediatric Research, Indiana University Simon Cancer Center (IUSCC), The Riley Hospital for Children, 1044 West Walnut Street, R3 302, Indianapolis, IN 46202-5525, USA

[§]Indiana University Simon Cancer Center, Indiana University School of Medicine, Indianapolis, IN

[‡]Department of Pharmacology and Toxicology, Indiana University School of Medicine, Indianapolis, IN

[†]Department of Biochemistry and Molecular Biology, Indiana University School of Medicine, Indianapolis, IN

[¶]Department of Medicine, Indiana University School of Medicine, Indianapolis, IN

[||]In Vivo Therapeutics Core, IUSCC, Indianapolis, IN

[⊥]Indiana University, School of Medicine, Department of Radiology and Imaging Sciences

Abstract

Objectives—The purpose of the present study was to develop and validate noninvasive bioluminescence imaging methods for differentially monitoring primary and abdominal metastatic tumor growth in mouse orthotopic models of pancreatic cancer.

Methods—A semiautomated maximum entropy segmentation method was implemented for the primary tumor region-of-interest, and a rule-based method for manually drawing a region-of-interest for the abdominal metastatic region was developed for monitoring tumor growth in orthotopic models of pancreatic cancer. The two region-of-interest methods were validated by having two observers independently segment Panc-1 tumors, and the results compared with the number of mesenteric lymph node nodules, and histopathological assessment of liver metastases. The findings were extended to orthotopic tumors of the more metastatic MIA PaCa-2 and AsPC-1 cells where separate groups of animals were implanted with different numbers of cells.

Corresponding authors: Dr. H.E. Shannon, FAX: (317) 274-8679, Phone: (317) 278-6422, heshanno@iu.edu. Dr. M.L. Fishel, FAX: (317) 274-8679, Phone: (317) 274-8810, mfishel@iu.edu.

Conflicts of Interest: The authors declare no conflicts of interest.

Results—The results demonstrated that the segmentation methods were highly reliable, reproducible and robust, and allowed statistically significant discrimination in the growth rates of primary and abdominal metastatic tumors of different cell lines implanted with different numbers of cells.

Conclusions—The present results demonstrate that primary tumors and abdominal metastatic foci in orthotopic pancreatic cancer models can be reliably quantified separately and noninvasively over time with bioluminescence imaging.

Keywords

Bioluminescence Imaging; Molecular Imaging; Pancreatic cancer; Metastases; ROI Segmentation; NSG Mice

Pancreatic ductal adenocarcinoma (PDAC) has a very poor prognosis and is currently the fourth leading cause of cancer death in the United States.[1] PDAC patients have a median survival of 6 months and a 5-year survival rate of 5%.[2,3] The lethal nature of PDAC is strongly associated with metastases to distant organs.[4,5] Rapid autopsy evaluation of patients who died of PDAC revealed that over 70% had metastases, most commonly to the liver and then lung.[6] Conventional approaches of surgical resection, radiation, and/or chemotherapy fail to prevent local recurrence and metastasis, most likely because of preexisting micrometastases at initial diagnosis.[4,7–9] Improved strategies for detecting, and ultimately treating, early and metastatic stages of the disease are therefore urgently needed, including in preclinical orthotopic models of pancreatic cancer.

Several approaches have been developed for assessing metastatic burden in preclinical models of pancreatic cancer. Zeidman et al.[10] pioneered the method of counting the number of metastases under a dissecting microscope at necropsy. Another approach has been to count the number of metastatic foci on histology sections.[e.g.,11] Rather than count individual metastatic foci, some investigations have simply reported the percentage of mice with visible foci.[e.g.,12–14] More recently, Hotz[15,16] developed a comprehensive dissemination score calculated based on the extent of local infiltration, distant metastases, and clinical signs of tumor burden. Studies using bioluminescence imaging (BLI), utilizing pancreatic cancer cells stably transfected with luciferase, have predominantly quantified only the primary or the whole body total tumor burden[17–21] *in vivo*. However, metastatic tumor burden has been quantified in several BLI studies after necropsy by homogenizing target tissues and measuring the bioluminescence signal *ex vivo*.[e.g.19] In addition, orthotopic models with pancreatic tumor cells stably transfected with fluorescent proteins have been used to monitor primary tumor growth *in vivo* and metastases at necropsy *ex vivo*.[22–24] While all of these approaches have provided valuable insights into pancreatic tumor biology and potential new treatment regimens, *ex vivo* approaches have the limitation of being invasive with respect to monitoring metastases, which requires the use of a relatively large number of animals since cohorts must be sacrificed at individual time points. The above *ex vivo* approaches also do not allow separate monitoring of primary tumor and metastases over time in individual animals. Methods for noninvasively monitoring primary and metastatic tumor growth differentially over time *in vivo* are needed to better understand not only the

dynamics of tumor growth of primary tumors and metastatic foci, but also to provide methods to monitor novel treatments over time in individual animals.

The purpose of the present study was to develop and validate noninvasive BLI methods for uniquely segmenting primary from metastatic tumors in mouse orthotopic models of pancreatic cancer in order to separately monitor primary and metastatic tumor growth noninvasively over time. A semiautomated maximum entropy[25,26] segmentation method was implemented for primary tumor region-of-interest (ROI) designation, and a rule-based method was developed for manually drawing and designating the ROI for the metastatic region. Both ROI methods were validated in the following manner. First, two observers independently segmented the images of the tumors of animals implanted orthotopically with the relatively less metastatic Panc-1 cells[14,21] expressing a luciferase-EGFP fusion protein. The results were compared with the number of mesenteric lymph node nodules counted following necropsy and histopathological assessment of liver metastases. We elected to utilize a relatively less aggressive cell line for validating the ROI methods based on the reasoning that it was necessary to determine whether relatively lower levels of metastases could be detected, and that this information would be informative in interpreting results on the appearance, or lack thereof, and growth rate of metastases with more aggressive cell lines. Second, the findings with Panc-1 cells were extended to orthotopic tumors of the more aggressive and metastatic MIA PaCa-2 and AsPC-1 cells where different groups of animals were implanted with different numbers of pancreatic cells to determine if the present segmentation methods allowed discrimination between the growth rates of different cell lines and implantation of different cell numbers. The results demonstrated that our segmentation methods were highly reproducible and relatively sensitive, allowing for statistically significant discrimination in the growth of the primary and metastatic tumors of different cell lines implanted with different cell numbers.

MATERIALS AND METHODS

Cell lines

Panc-1, AsPC-1 and MIA PaCa-2 cells were purchased from American Type Culture Collection and cultured as instructed by the vendor. The cell lines were analyzed by IDEXX RADL (Columbia, MO) and the authenticity of each line was confirmed to be human, have no cross-contamination, and correct at the molecular level via microsatellite marker analysis.

Transduction of cell lines with lentiviral vectors expressing luciferase/fluorescent protein fusion proteins

Panc-1 cells were transduced with the lenti viral vector pCL6LucEGwo containing a fusion protein of the human codon usage-optimized luciferase cDNA (InvivoGen, San Diego, CA) and the cDNA for the enhanced green fluorescent protein (Clontech). AsPC-1 and MIA-PaCa-2 cells were transduced with the lentiviral vector pCL6LucCHwo which contains a fusion protein of the human codon usage-optimized luciferase cDNA and the cDNA for mCherry (Clontech). Details on the vector and cloning will be available elsewhere (Wiek, Hanenberg, Pollok, unpublished). The fusion mRNA is expressed off a modified promoter from the U3 region of the SFFV retrovirus.[27] Replication-incompetent infectious lentiviral

particles in the vesicular stomatitis virus glycoprotein (VSV-G) pseudotype (kindly obtained from Dirk Lindemann, Dresden, Germany) were generated using 293T cells as previously described[27] and high viral titers were obtained (~10^9 transduction units per ml). Cell lines were transduced one time with frozen supernatants at a multiplicity-of-infection (MOI) of 100 in the presence of 8 μg/ml polybrene and analyzed for EGFP (Panc-1) or mCherry (MIA PaCa-2, AsPC-1) expression by flow cytometry (BD LSR Cell Analyzer, BD Biosciences, San Jose, CA).

Chemicals

D-Luciferin-K^+ (Caliper Lifescience USA) was prepared in phosphate buffered saline to yield a final concentration of 20 mg/ml (pH 7), and was stored in individual light tight aliquots at −20°C until use.

Animals

All studies were carried out in accordance with, and approval of, the Institutional Animal Care and Use Committee of Indiana University School of Medicine, and the Guide for the Care and Use of Laboratory Animals.[28] Male and female NOD.Cg-*Prkdc*^{scid} Il2rg^{tm1Wjl}/SzJ (NSG) mice were obtained from the In Vivo Therapeutics Core of the Indiana University Simon Cancer Center. Animals were maintained under pathogen-free conditions and maintained on Teklad Lab Animal Diet (TD 2014, Harlan Laboratories USA) with *ad libitum* access to sterile tap water under a 12-hour light-dark cycle at 22–24 °C.

Survival surgery

Mice were anesthetized with 5% isoflurane in oxygen. An incision (1–1.5 cm) was created in the left abdominal flank under aseptic conditions. The pancreas was carefully exposed and 50 μl of cell solution in phosphate buffered saline were injected into the tail of the pancreas as previously described[29] (Panc-1: 2×10^6 cells, N = 34; MIA PaCa-2 and AsPC-1: 2×10^4 or 2×10^5 cells, N = 6/group). The peritoneum and fascia were closed in separate layers using a continuous 4/0 Prolene suture; the skin wound was closed using a wound clip.

In vivo Imaging

Beginning on day 7 post tumor implantation and continuing weekly thereafter, dynamic bioluminescence images were acquired using a Berthold NightOwl (BL981, Berthold Technologies Inc. USA) imaging system outfitted with a 24W inductive header (RH-7, Zoo Med Laboratories Inc.) and a custom anesthesia manifold supporting up to 3 mice per session. Prior to imaging, the skin over the abdomen and left lateral epigastric regions were shaved and depilated with Nair (Church and Dwight Inc., USA). Anesthetic induction was achieved with 2–4% isoflurane, and animals were administered D-luciferin (150 mg/kg) subcutaneously. Mice were immediately transferred to the heated stage (40±1 °C) of the Imager, placed on their backs, and sequentially imaged at 2 min intervals for 40 mins with image integration times ranging from 1 to 120 sec/image. At the completion of the sequence, anatomical reference photos were acquired permitting generation of fused image sets.

In order to validate the ROI methods (see *Image Analysis*), 34 mice with Panc-1 orthotopic tumors were utilized. All mice were imaged on day 7 or 8 (i.e., baseline) after implant and then block randomized (using a random number list), by flux density at the time of peak light emission in the primary ROI, to imaging groups to balance the initial tumor burden of the primary tumors across groups. One animal was excluded from the study due to lack of signal above background at baseline (final N = 33). One group of nine mice was imaged weekly to monitor changes in tumor burden over time in the same animals. Additional separate groups of 6 mice each were imaged only once, on day 7 or 8, 14, 20 or 28, and then necropsied the following day. When prominent metastases had not yet developed by day 28, the original design was modified in order to allow time for metastases to develop and the remaining 9 mice, rather than being imaged on day 35, were randomly assigned to be imaged on either day 43, 50 or 57 (3/day), and necropsied the following day.

Following necropsy, the number of mesenteric lymph node metastatic nodules was counted and *ex vivo* GFP imaging using a Bright Light System Illumatool LT9900 (LightTools Research, Encinitas, CA) was used to visualize primary tumor and metastases. The livers were then fixed in 10% neutral buffered formalin for at least 24 hours and then embedded in paraffin, sectioned, and stained with H&E and Ki67 using standard immunohistochemical techniques and 3,3′-diaminobenzadine as chromagen. Morphometric analysis of Ki67 staining was done with an Aperio Whole Slide Imaging System (Aperio Technologies, Vista, CA) using the Aperio software Positive Pixel Count Algorithm under the supervision of a board certified pathologist. Images of stained sections were captured with ImageScope v11.2.0.780 (Aperio Technologies). We also sought to determine if the method could be used to monitor more aggressive tumors, and to detect differences in tumor burden due to implantation of different numbers of cells. The orthotopic model described above with Panc-1 cells was again utilized. Groups of 6 mice each were implanted orthotopically with 2×10^4 or 2×10^5 AsPC-1 or MIA PaCa-2 cells; one mouse implanted with 2×10^4 MIA PaCa-2 cells died perioperatively for a final N of 5 for this group. Mice were imaged weekly for up to 8 weeks to monitor changes in primary and metastatic tumor burden over time in the same animals. For these studies, mice were placed on their sides for the first image on day 7 in order to better image the primary tumor; thereafter, they were placed on their backs and the ventral surface imaged. Thus, the baseline scan for the primary tumor of these animals was day 7, and for the metastases it was day 14.

Image Analysis

To provide visualization, segmentation and time series quantification from the 40-min scan, BLI and anatomical reference images were imported into custom-developed software. Pseudo-colored parametric overlays of BLI time-series with anatomical reference images were dynamically constructed for each animal. Using the image of the time series with the peak light emission for each individual animal, ROIs were designated for both primary tumors and a metastatic region. Primary tumors were segmented through time using the semi-automated maximum entropy ROI algorithm.[25] For metastatic tumors, ROIs of the abdomen were manually drawn which encompassed the dome of the liver and extended to the animal's inferior inguinal aspect which included the genitals (see also Fig. 1). To avoid photon spillover from the primary to the metastasis ROI (and *vice versa*), the manual ROIs

maintained an approximate 3 mm offset from the primary tumor on all lateral aspects across all 20 imaging time points. Occasionally (particularly when tumors were small) gastrointestinal motility resulted in movement of the tumor. When gastrointestinal motility-induced (or rarely, animal motion-induced) movement of the primary tumor occurred, the manual ROIs were adjusted to maintain a 3 mm offset from any location of the primary on any of the 20 BLI imaging frames. The extracted time series were then analyzed for total emission flux (Ph/sec), average emission flux density (Ph/sec*mm^2) and area (mm^2) at the peak of the time course kinetics according to:

$$I_T(n,t)=\sum_{i=1}^{m} I_p(i,t) \quad (1)$$

$$I_A(n,t)=\frac{I_T(n,t)}{m} \quad (2)$$

$$D_A(n)=\max[I_A(n,t)] \quad (3)$$

$$F_T(n)=D_T(n)*A(n) \quad (4)$$

where I_T, I_p, n, m, I_A and t are the total emission flux density (Ph/s*mm^2), pixel emission flux density, subject, total number of pixels, average emission flux density, and time points, respectively. Moreover, D_A, F_T and A are the average emission flux density, total emission flux at the peak of the time course, and ROI area, respectively. To minimize the role of tumor and animal motion on time course parameters, individual ROIs across image frames were aligned by computing the per frame center of gravity[30] offset between successive frames, and applying the x-y offset to the ROI prior to computing I_T or I_A described in equations 1 or 2, respectively.

Data Analysis

Each ROI was independently constructed by two observers (BPM and HES). The interobserver reliability of the measurements was determined by Pearson product-moment correlations. To evaluate if the difference between pairs of measurements increased as the mean of the pairs increased, the correlation between the two values was determined with a homoscedasticity plot;[31] differences were not correlated with mean values when transformed logarithmically, as recommended.[31,32] In order to determine the reproducibility of the measurements, the coefficients of variation were calculated for each animal for each pair of images; the coefficient of variation was calculated as the ratio of the standard deviation of the log of the two ROI measurements to the mean of the log of the two ROI measurements. Limits of agreement (Bland-Altman) plots[31] were constructed from the logarithmically transformed data, and the limits of agreement calculated[31,32] according to:

$$LOA=\left|\left(\frac{SD_D}{\overline{X}_G}\right)*1.96*100\right| \quad (5)$$

where LOA, SD_D, and $\bar{X}_G$ are the limits of agreement, standard deviation of the difference, and grand mean respectively. Tumor volumes/bioluminescence signals, ROI areas and the number of lymph node nodules were analyzed by a 1- or 2-way ANOVA, as appropriate, using SigmaPlot 11.2 (Systat Software, Inc).

RESULTS

Visualization of abdominal metastases

Abdominal metastases were typically not readily visible on standard BLI images until foci were relatively large in size (see Fig. 1 and also Fig 6). However, the visualization of the bioluminescence signal from the abdominal metastases could be enhanced by adjusting the manner in which the pseudocolor was mapped to the photon flux density scale (see Fig. 1A1 and A2). The adjustment was accomplished by compressing the color scale so that lower flux densities were represented by “higher/brighter” colors, or to a color rather than ‘no color’, on the fused overlays of the BLI signal on the anatomical images. Following adjustment of the color mapping, bright spots of smaller metastatic foci became visible, and disseminated micrometastases were visible as diffuse coloring (Fig. 1A2). With these considerations in mind, we sought to quantitate the bioluminescence signals in the primary and metastasis ROIs.

Validation of ROI methods in Panc-1 orthotopic tumors

The primary tumor and abdominal metastases increased over time in mice with Panc-1 orthotopic tumors as measured by bioluminescence (Fig. 2; see also Fig. 6A). We initially examined the total flux in each region. Total flux is the sum of the light emitted from all of the luciferase expressing cells in a region, and is indicative of the total number of cells in a region, regardless of whether those cells are widely dispersed or clustered together. When the data were expressed as the total photon flux (Ph/sec) in the ROIs for the primary tumor and metastases (Fig. 2A), the total flux within the metastasis ROI was larger in magnitude than the total flux from the primary tumor ROI, at times by as much as several orders of magnitude, indicating that there were more luciferase expressing cells in the metastasis ROI than in the primary ROI. Total flux was statistically significantly larger in magnitude for the metastases than for the primary as indicated by a significant main effect for Tumor ROI ($F_{(1,164)} = 176.5$, $p < 0.001$; two-way ANOVA). The total flux of both primary and metastatic tumors increased over time as indicated by a significant main effect for Days ($F_{(6,164)} = 56.7$, $p < 0.001$; two-way ANOVA). Further, the slopes of the growth curves for the primary and metastatic tumors were different as indicated by a significant Tumor ROI x Day interaction ($F_{(6,164)} = 36.7$, $p < 0.001$; two-way ANOVA). We also compared luciferase-EGFP fusion protein expressing PANC-1 cells and the parental cells on the rate of tumor growth and metastatic tumor progression, and did not find significant differences (data not shown), indicating that ectopic expression of this fusion protein did not affect the potential of tumor growth and metastases in PANC-1 cells.

As expected, the area (in mm^2) of the ROIs for the primary tumors significantly increased over days post implantation (mean±SD across all days: 23.9±16.9 mm^2) as evidenced by a significant main effect for days ($F_{(7,81)} = 10.6$, $p < 0.001$; one-way ANOVA), whereas the

areas of the ROIs for the metastases were constant over days (1167±111 mm^2) as evidenced by a non-significant main effect for Days ($F_{(7,81)} = 1.9$, $p > 0.05$; one-way ANOVA). To examine the average amount of light emitted per unit of area in both regions, indicative of the compactness or density of the light-emitting cells, the data were expressed as the average flux density (Ph/sec*mm^2) within the ROIs. In contrast to the findings with total flux, the density of the flux within the smaller primary tumor ROI was larger in magnitude than the density of the flux from the larger metastases ROI (Fig. 2B), by as much as several orders of magnitude. That is, although there were substantially fewer total photons emitted from the primary than the metastatic region, there were more photons per mm^2 emitted from the primary region compared with the metastatic region, consistent with the cells in the primary tumor being clustered much more closely together than in the metastatic region. Flux density was statistically significantly larger in magnitude in the primary than the metastatic ROI ($F_{(1,164)} = 248.4$, $p < 0.001$; two-way ANOVA). Moreover, the flux density of both primary and metastatic tumors increased over time as indicated by a significant main effect for Days ($F_{(6,164)} = 39.0$, $p < 0.001$; two-way ANOVA). In addition, the slopes of the growth curves measured by flux density for the primary and metastatic tumors were significantly different as indicated by a significant Tumor ROI x Day interaction ($F_{(6,164)} = 34.5$, $p < 0.001$; two-way ANOVA).

Metastatic burden was also monitored following necropsy of animals at each time point and counting the number of mesenteric lymph node nodules, histopathological assessment of liver sections, and visualization of GFP intensity in livers. The number of lymph node nodules increased over time (Fig. 2C; $F_{(6,32)} = 21.0$, $p < 0.001$), and the number of nodules was significantly increased on days 50 and 57 ($p < 0.05$, Dunnett's test vs Day 7). In comparison, the total photon flux in the metastases ROI was significantly increased from day 29 post implantation onwards (Fig. 2A). Livers from animals imaged on day 29 and then necropsied were assessed to be normal upon histopathological assessment, but focal and multifocal metastases increased thereafter, with the size of metastases ranging from approximately 8 to 10 cells to as many as approximately 150 cells/metastasis, and with increasing Ki67 index values (data not shown and Fig. 3A, B), concordant with the BLI data. Similarly, visualization of GFP expression indicated no apparent metastases on day 29 but increasing abundance of metastases through day 57 post-implant (Fig. 3C), again concordant with the BLI data.

The interobserver reliability of the measurements was determined by Pearson product-moment correlations (Fig. 4). Total flux and flux density from ROIs for the primary tumors, constructed using the semi-automated maximum entropy algorithm,[25] were highly concordant ($r = 0.999$ and $r = 0.997$, respectively) between the two observers (Fig. 4A,C). Moreover, total flux and flux density from ROIs for the metastases, constructed manually, were also highly concordant ($r = 0.988$ and $r = 0.992$; Fig. 4B, D). In addition, the slopes of the correlations were very close to 1.0, indicating that the two observers were also in close agreement.

Absolute reliability is the degree to which repeated measurements vary for individuals and can be measured using the coefficient of variation and limits of agreement.[31,32] The coefficients of variation for the total photon flux (Ph/sec) were approximately 0.19 and 0.20

for the primary and metastases, and were approximately 0.05 and 0.20, respectively, for the photon flux density (Ph/sec*mm^2), indicating an acceptably small dispersion in the data. The agreement between the ROIs of the two observers was also quantified from Bland-Altman plots (Fig. 5). For both the primary and metastases ROIs, the bias, or average difference between the two observers, was relatively negligible (Fig. 5, dotted lines) and was approximately 0.028 and 0.016 log units for the total flux and flux density for the primary tumor ROIs, and was approximately 0.040 and 0.024 log units, respectively, for the metastases ROIs. Limits of agreement are expected to contain the difference between two measurements for 95% of pairs of future measurements on similar individual subjects.[31] The limits of agreement values were approximately 3.5% and 2.3% for the total photon flux (Ph/sec) for the primary and metastases measurements, and 1.5% and 4.9% for the photon flux density (Ph/sec*mm2) measurements. Taken together, the present findings indicate that the ROI segmentation methods developed in the present study for constructing ROIs for the primary pancreatic tumor and abdominal metastases are valid, reproducible, and reliable.

MIA PaCa-2 and AsPC-1 orthotopic tumors

We next sought to extend the findings with Panc-1 cells to orthotopic tumors of the more aggressive and metastatic MIA PaCa-2 and AsPC-1 cells to determine if the present segmentation methods allowed discrimination between the growth rates of different cell lines and implantation of different cell numbers.

In mice with MIA PaCa-2 orthotopic tumors, the primary tumor and metastases increased over time after implantation with either 2×10^4 or 2×10^5 cells (Fig. 6B and Fig. 7), and with a cell number-related decrease in survival (Table 1). MIA PaCa-2 cells grew more rapidly, compared with Panc-1 cells, and also produced a cell number-related decrease in survival (Table 1). When the data were expressed as total flux (Ph/sec), there was a significant increase across days both for the primary tumor ($F_{(6,64)} = 3.9$, $p = 0.002$) and metastases ($F_{(5,54)} = 25.8$, $p < 0.001$). Moreover, the overall difference in the magnitude of the signals between the two cell numbers (2×10^4 or 2×10^5 cells per mouse) implanted for the primary tumor was not significant ($F_{(1,64)} = 3.2$, $p = 0.08$; Fig. 7A) but was statistically significant for the metastases ($F_{(1,54)} = 63.9$, $p < 0.001$; Fig. 7B). Post-hoc analyses, however, indicated that growth of the primary tumors was significantly greater than baseline on day 42 for the group of mice implanted with 2×10^5 cells (Fig. 7A). Further, on days 35 and 42, the BLI signal of the metastases was significantly different from the baseline (Fig. 7B). When the data were expressed as the average density of the flux (Ph/sec*mm^2), there was again a significant increase across days both for the primary tumor ($F_{(6,64)} = 17.0$, $p < 0.001$; Fig. 7C) and metastases ($F_{(5,54)} = 13.3$, $p < 0.001$; Fig. 7D). The overall difference in signal for the two cell numbers implanted was significantly different for the primary tumor ($F_{(1,64)} = 12.4$, $p < 0.001$; Fig. 7C) as well as for the metastases ($F_{(1,54)} = 24.6$, $p < 0.001$; Fig. 7D). Post-hoc analyses indicated that for flux density, the primary tumor was significantly increased from baseline on days 49 – 56 for the 2×10^4 cells group and on days 29 – 42 for the 2×10^5 cells group (Fig. 7C). In comparison, on days 35 – 42 for the 2×10^5 cells group, flux density for the metastases was significantly different from baseline; however, for the group of mice implanted with 2×10^4 cells, no significant difference from baseline was observed on any day (Fig. 7D). Analyses of inter-observer reliability,

coefficients of variation, and limits of agreement for MIA PaCa-2 orthotopic tumors were similar to those for Panc-1 orthotopic tumors (data not shown). The present data with MIA PaCa-2 orthotopic pancreatic tumors demonstrate that our segmentation methods can discriminate between the growth rates of different numbers of cells implanted, and that flux density is the superior measure for primary tumors while total flux is the superior measure for metastases.

In mice with AsPC-1 orthotopic tumors, the primary tumor and metastases again increased over time after implantation with either 2×10^4 or 2×10^5 cells (Fig. 6C and Fig. 8). AsPC-1 cells grew more aggressively than either Panc-1 or MIA PaCa-2 tumors, with a greater cell number-related decrease in survival than Panc-1 or MIA PaCa-2 (Table 1). When the data were expressed as total flux (Ph/sec), there was a significant increase across days both for the primary tumor ($F_{(5,46)} = 7.1$, $p < 0.001$) and metastases ($F_{(4,37)} = 11.8$, $p < 0.001$). Moreover, the overall difference in the magnitude of the signals between the two cell numbers was significant for both the primary tumor ($F_{(1,46)} = 15.8$, $p < 0.001$; Fig. 8A) as well as for the metastases ($F_{(1,37)} = 7.1$, $p = 0.012$; Fig. 8B). Post-hoc analyses indicated that growth of the primary tumors measured by total flux was not significantly different from baseline on any day for the 2×10^4 cells group but was significantly different from baseline on day 42 for the 2×10^5 cells group (Fig. 8A). Further, growth of the metastases was significantly different from the baseline scan on day 42 for the 2×10^4 cells group and on days 35 – 42 for the 2×10^5 cells group (Fig. 8B). In contrast, when the data were expressed as the density of the flux (Ph/sec*mm^2), there was a significant increase across days both for the primary ($F_{(5,46)} = 51.1$, $p < 0.001$) and metastases ($F_{(4,37)} = 10.7$, $p < 0.001$). In addition, the overall difference in signal for the two cell numbers implanted was significantly different for the primary tumor ($F_{(1,46)} = 7.3$, $p = 0.01$; Fig. 8C) as well as for the metastases ($F_{(1,37)} = 4.2$, $p = 0.048$; Fig. 8D). Post-hoc analyses indicated that for flux density, the primary tumor was significantly different from baseline on day 42 for the 2×10^4 cells group and on days 29 – 42 for the 2×10^5 cells group (Fig. 8C, D). In comparison, flux density for the metastases was not significantly different from the baseline on any day for the 2×10^4 cells group but was significant on day 42 for the 2×10^5 cells group (Fig. 8C, D). Analyses of interobserver reliability and limits of agreement for AsPC-1 orthotopic tumors were similar to those for Panc-1 and MIA PaCa-2 orthotopic tumors (data not shown). The present data with AsPC-1 orthotopic pancreatic tumors provide further confirmation that the segmentation methods used here discriminate the growth rates of different cell lines, and also confirms that these methods can discriminate the growth rates of different numbers of cells implanted. Our data with AsPC-1 tumors also confirm that flux density is the superior measure of the relatively more compacted primary tumors while total flux is the superior measure of the relatively more dispersed metastases.

DISCUSSION

Current approaches for assessing metastatic growth in preclinical orthotopic models of pancreatic cancer largely rely on quantification of metastases after necropsy, which can require large numbers of animals and precludes investigation of metastatic growth over time, and/or following pharmacologic or other treatments within individual animals. In the present study, we developed strategies for longitudinally and noninvasively monitoring primary and

metastatic tumor burden separately by BLI. We demonstrated that a primary tumor ROI can be reliably constructed using a semi-automated maximum entropy algorithm.[25] Further, we demonstrated that a metastasis ROI, inclusive of the entire abdomen but exclusive of an approximately 3 mm region around the primary ROI, can be reliably constructed manually. The present results demonstrated that, utilizing these ROIs, primary and metastatic tumor burden can be noninvasively monitored longitudinally, and, the approach is sensitive enough to distinguish growth rates of orthotopic tumors not only between cell lines, but also between tumors initiated by implantation of different numbers of cells.

We utilized several measures of reliability and reproducibility in the present study. The interobserver reliability was assessed by correlation of the ROI signals constructed independently by two observers. The correlation coefficients were generally greater than 0.99, indicating a very high degree of reliability, and, the slopes of the correlations were close to 1.0, indicating good agreement between the two observers. The absolute reliability of the ROI measurements, as assessed by the coefficient of variation on logarithmically transformed data, ranged from approximately 0.05 to 0.20, which was well within acceptable limits. The limits of agreement, expected to contain the difference between two measurements for 95% of pairs of future measurements on similar individual subjects,[31] was also within acceptable limits (1.5%– 5%) when the data were logarithmically transformed. The need to transform the data was not unexpected: as previously noted,[32] it is common for the variability in biological data to increase as the magnitude of the mean increases. Intuitively, this is due to numbers closer to zero tending to cluster together more closely, while numbers further from zero are generally less closely clustered. Thus, we conclude that the methods of segmentation of primary and metastatic tumor burden presented herein are reliable and reproducible.

Data from BLI studies may be expressed either as total luminance flux in the ROI, expressed as Ph/sec, or as luminance flux density in the ROI, expressed as photons/sec/unit of area. Both methods of expression have biological significance. Total flux aggregates the photons emitted from dispersed cells expressing luciferase, whereas flux density can indicate the localized density of cells expressing luciferase. In the present studies, we found that the primary tumor appears to be best visualized and analyzed when data are expressed as the density of the BLI signal. The present finding is consistent with the primary tumor being localized in a relatively small area and thus it is primarily the density of the tumor cells and their photon emission that changes over time with growth, even though the total number of photons may be relatively small in magnitude. On the other hand, we found that the metastasis burden appears to be best visualized and analyzed by the total flux, thereby aggregating, or summating, the more diffuse signals from small clusters of cells as occurs in metastatic disease. It is the spread of relatively small clusters of metastatic tumor cells that primarily changes over time more so than density. Studies are in progress to assess this innovative analysis methodology in the context of conventional and novel treatments for pancreatic cancer.

In the present study, we found that the total bioluminescence signal (in Ph/sec) in the metastases ROI was as much as several orders of magnitude larger than the signal from the primary tumor ROI. It is not uncommon for studies to use whole body BLI to monitor what

is generally interpreted as primary tumor growth. However, the present data indicate that such an interpretation could be incorrect and potentially misleading. Rather, the signal from whole body imaging is a mixture of signal from the primary tumor and the metastases, and the signal from the metastases has the potential to overwhelm the signal from the primary when measured as total photon flux (in Ph/sec). This observation is consistent with the observation of Graeser and coworkers[19,20] who previously suggested that with whole body BLI (using MIA PaCa-2 and AsPC-1 orthotopic models), the signal from the abdominal metastases can disproportionately contribute to the overall bioluminescence signal, and can contribute to the signal ascribed to the primary tumor. Taken together, these observations indicate that bioluminescence data from whole body imaging without segmentation, particularly when both primary tumor and metastases are present, should be interpreted with caution.

The present findings directly comparing the growth rates and metastatic potential of orthotopically implanted Panc-1, MIA PaCa-2 and AsPC-1 pancreatic cancer cell lines extend previous findings with these cell lines. Loukopoulos et al.[14] directly compared the tumorigenicity and rate of metastasis of 10 different pancreatic cell lines, including Panc-1 and AsPC-1, after orthotopic implantation in NSG mice. The AsPC-1 cell line was somewhat more tumorigenic and produced a larger percentage of animals with peritoneal dissemination and lymph node metastases than did Panc-1 cells when animals were necropsied at time of morbidity or 100 days after implantation, consistent with the present findings in NSG mice. Torgenson et al.[33] found that implantation of 1×10^6 MIA PaCa-2 and AsPC-1cells had similar growth characteristics at 2 and 5 weeks after orthotopic injection in nude mice (Ncr-Nu/Nu), whereas we found that AsPC-1 cells were somewhat more aggressive than MIA PaCa-2 cells in NSG mice. Further, Hotz et al.[16] found that orthotopic injection of AsPC-1 cells resulted in 100% tumor development, whereas injection of MIA PaCa-2 cells resulted in 83% tumor take and progression of disease, consistent with the present results. Although differences in methodology, e.g., number of cells injected, indicate that comparisons among studies should be interpreted with caution, the data taken together suggest that AsPC-1 cells are at least somewhat more tumorigenic and have a higher rate of metastases than MIA PaCa-2 and Panc-1 cells when implanted into the pancreas. Most importantly, from this study we show that we are able to detect, and quantify differences, in primary tumor growth and distant metastases for these 3 pancreatic cancer cell lines non-invasively over time with reliability and reproducibility. In the present study, an area of at least 3 mm around the primary tumor was excluded from both the primary and metastases ROIs to avoid counting photons emitted from the primary tumor in the metastases ROI (and vice versa). This region likely contains tumor cells, but signal from these were not included in the present analyses. Whether the cells in this region should be excluded to avoid cross-contamination of signals, included with the primary as a growth edge, included with the metastases, or considered as a separate localized infiltration region is a topic for future studies specifically designed to address this question from imaging as well as histological and other approaches. In addition, the total flux in the metastases ROI was likely underestimated, in part due to the 3 mm border around the primary, but also because we chose to exclude from the metastases ROI any portion of the abdomen into which the primary moved. Nevertheless, the occurrence and growth of metastases was reliably

measured in the present study, and the underestimation of the total flux of the metastasis region does not appear to have been a substantive issue.

In summary, the present study demonstrated that primary tumors and abdominal metastatic foci in orthotopic pancreatic cancer models can be reliably monitored and quantified separately and noninvasively over time with bioluminescence imaging. A semiautomated maximum entropy segmentation method was validated for primary tumor ROI designation. A rule-based method for manually drawing and designating the ROI for the metastatic region was also validated. The results of the present study demonstrated that the present segmentation methods were not only highly reliable, reproducible and robust but also relatively sensitive, allowing statistically significant discrimination in the growth rates of the primary and metastatic tumors of different cell lines implanted with different numbers of cells. The novel segmentation methods reported here will facilitate investigations of the biology of primary and metastatic tumor growth, as well as the effects of novel treatments, over time in individual animals.

Acknowledgments

Sources of Funding: This work was supported in part by National Cancer Institute (NCI) grants CA16791 (MLF and MRK), CA-R37-075059 (MK), CA155086 (XJ) and by the Pancreatic Cancer Signature Center, the Indiana University CTSI P3 program, Hope on Wheels (MRK), the Riley Children's Foundation (MRK) and the Indiana University CTSI (MRK).

References

1. Siegel R, Naishadham D, Jemal A. Cancer statistics, 2013. CA Cancer J Clin. 2013; 63:11–30. [PubMed: 23335087]
2. Wray CJ, Ahmad SA, Matthews JB, et al. Surgery for pancreatic cancer: recent controversies and current practice. Gastroenterology. 2005; 128:1626–1641. [PubMed: 15887155]
3. Jemal A, Siegel R, Ward E, et al. Cancer statistics, 2009. CA Cancer J Clin. 2009; 59:225–249. [PubMed: 19474385]
4. Jemal A, Siegel R, Ward E, et al. Cancer statistics, 2007. CA Cancer J Clin. 2007; 57:43–66. [PubMed: 17237035]
5. Hidalgo M. Pancreatic cancer. N Engl J Med. 2010; 362:1605–1617. [PubMed: 20427809]
6. Iacobuzio-Donahue CA, Fu B, Yachida S, et al. DPC4 gene status of the primary carcinoma correlates with patterns of failure in patients with pancreatic cancer. J Clin Oncol. 2009; 27:1806–1813. [PubMed: 19273710]
7. Allison DC, Piantadosi S, Hruban RH, et al. DNA content and other factors associated with ten-year survival after resection of pancreatic carcinoma. J Surg Oncol. 1998; 67:151–159. [PubMed: 9530884]
8. Burris HA 3rd. Recent updates on the role of chemotherapy in pancreatic cancer. Semin Oncol. 2005; 32:S1–3. [PubMed: 16143160]
9. Yeo TP, Hruban RH, Leach SD, et al. Pancreatic cancer. Curr Probl Cancer. 2002; 26:176–275. [PubMed: 12399802]
10. Zeidman I, Mc CM, Coman DR. Factors affecting the number of tumor metastases; experiments with a transplantable mouse tumor. Cancer Res. 1950; 10:357–359. [PubMed: 15420702]
11. Tomioka D, Maehara N, Kuba K, et al. Inhibition of growth, invasion, and metastasis of human pancreatic carcinoma cells by NK4 in an orthotopic mouse model. Cancer Res. 2001; 61:7518–7524. [PubMed: 11606388]

12. Gaspar NJ, Li L, Kapoun AM, et al. Inhibition of transforming growth factor beta signaling reduces pancreatic adenocarcinoma growth and invasiveness. Mol Pharmacol. 2007; 72:152–161. [PubMed: 17400764]
13. Ramachandran V, Arumugam T, Wang H, et al. Anterior gradient 2 is expressed and secreted during the development of pancreatic cancer and promotes cancer cell survival. Cancer Res. 2008; 68:7811–7818. [PubMed: 18829536]
14. Loukopoulos P, Kanetaka K, Takamura M, et al. Orthotopic transplantation models of pancreatic adenocarcinoma derived from cell lines and primary tumors and displaying varying metastatic activity. Pancreas. 2004; 29:193–203. [PubMed: 15367885]
15. Hotz HG, Reber HA, Hotz B, et al. An improved clinical model of orthotopic pancreatic cancer in immunocompetent Lewis rats. Pancreas. 2001; 22:113–121. [PubMed: 11249064]
16. Hotz HG, Reber HA, Hotz B, et al. An orthotopic nude mouse model for evaluating pathophysiology and therapy of pancreatic cancer. Pancreas. 2003; 26:e89–98. [PubMed: 12717279]
17. Medicherla S, Li L, Ma JY, et al. Antitumor activity of TGF-beta inhibitor is dependent on the microenvironment. Anticancer Res. 2007; 27:4149–4157. [PubMed: 18229422]
18. McNally LR, Welch DR, Beck BH, et al. KISS1 over-expression suppresses metastasis of pancreatic adenocarcinoma in a xenograft mouse model. Clin Exp Metastasis. 2010; 27:591–600. [PubMed: 20844932]
19. Bornmann C, Graeser R, Esser N, et al. A new liposomal formulation of Gemcitabine is active in an orthotopic mouse model of pancreatic cancer accessible to bioluminescence imaging. Cancer Chemother Pharmacol. 2008; 61:395–405. [PubMed: 17554540]
20. Graeser R, Bornmann C, Esser N, et al. Antimetastatic effects of liposomal gemcitabine and empty liposomes in an orthotopic mouse model of pancreatic cancer. Pancreas. 2009; 38:330–337. [PubMed: 19142174]
21. Muniz VP, Barnes JM, Paliwal S, et al. The ARF tumor suppressor inhibits tumor cell colonization independent of p53 in a novel mouse model of pancreatic ductal adenocarcinoma metastasis. Mol Cancer Res. 2011; 9:867–877. [PubMed: 21636682]
22. Katz MH, Takimoto S, Spivack D, et al. An imageable highly metastatic orthotopic red fluorescent protein model of pancreatic cancer. Clin Exp Metastasis. 2004; 21:7–12. [PubMed: 15065597]
23. Grzesiak JJ, Tran Cao HS, Burton DW, et al. Knockdown of the beta(1) integrin subunit reduces primary tumor growth and inhibits pancreatic cancer metastasis. Int J Cancer. 2011; 129:2905–2915. [PubMed: 21491421]
24. Bouvet M, Wang J, Nardin SR, et al. Real-time optical imaging of primary tumor growth and multiple metastatic events in a pancreatic cancer orthotopic model. Cancer Res. 2002; 62:1534–1540. [PubMed: 11888932]
25. Sin, CF.; Leung, CK. Image segmentation by edge pixel classification with maximum entropy. IEEE Xplorer; Proceedings of the International Symposium on Intelligent Multimedia, Video and Speech Processing; 2001. p. 283-286.
26. Gu D, Liu H, Su GH, et al. Combining hedgehog signaling inhibition with focal irradiation on reduction of pancreatic cancer metastasis. Mol Cancer Ther. 2013; 12:1038–1048. [PubMed: 23468532]
27. Leurs C, Jansen M, Pollok KE, et al. Comparison of three retroviral vector systems for transduction of nonobese diabetic/severe combined immunodeficiency mice repopulating human CD34+ cord blood cells. Hum Gene Ther. 2003; 14:509–519. [PubMed: 12718762]
28. Guide for the Care and Use of Laboratory Animals. 8. The National Academies Press; 2011.
29. Bruns CJ, Harbison MT, Kuniyasu H, et al. In vivo selection and characterization of metastatic variants from human pancreatic adenocarcinoma by using orthotopic implantation in nude mice. Neoplasia. 1999; 1:50–62. [PubMed: 10935470]
30. van Assen HC, Egmont-Petersen M, Reiber JH. Accurate object localization in gray level images using the center of gravity measure: accuracy versus precision. IEEE Trans Image Process. 2002; 11:1379–1384. [PubMed: 18249706]
31. Bland JM, Altman DG. Statistical methods for assessing agreement between two methods of clinical measurement. Lancet. 1986; 1:307–310. [PubMed: 2868172]

32. Atkinson G, Nevill AM. Statistical methods for assessing measurement error (reliability) in variables relevant to sports medicine. Sports Med. 1998; 26:217–238. [PubMed: 9820922]

33. Torgenson MJ, Shea JE, Firpo MA, et al. Natural history of pancreatic cancer recurrence following “curative” resection in athymic mice. J Surg Res. 2008; 149:57–61. [PubMed: 18222475]

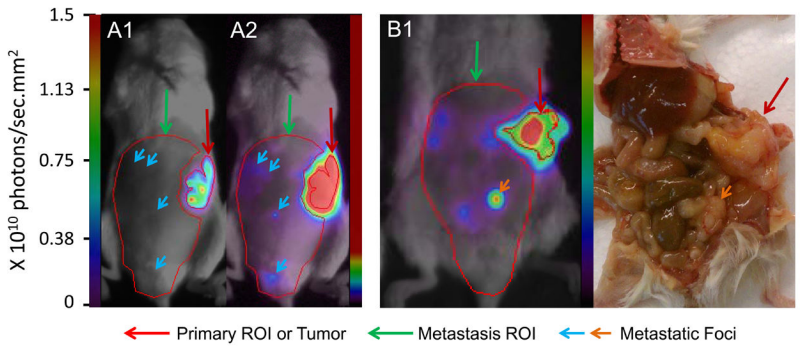

Figure 1.

(A1 and A2) Illustration of ROIs and color mapping for primary and abdominal metastatic regions of bioluminescence images in an animal implanted orthotopically with Panc-1 cells and imaged 34 days post implant. In A1, the pseudocolor was mapped to the photon flux density scale using a typical rainbow scale where the highest flux density in the image was mapped to red, and the color transitioned through the colors of the rainbow, and then to 'no color' (i.e., transparent on the fused overlay of the BLI image on the anatomical image, thus allowing the anatomical image to be seen) as the flux density decreased (see scales to the left of A1). With this color mapping approach, the magnitudes of the photon flux densities in the metastatic foci and micrometastases were too small to be mapped to a color, and therefore were not visible, until a focus become relatively large (see B). In order to enhance the visibility of metastases, in A2 the color mapping to the flux density scale was compressed to approximately 18% of full scale, such that 0 – 18% of the full flux density scale was mapped to rainbow color transitions, and 18 – 100% of full scale was mapped to red (see color scale to the right of A2). The flux density scales are the same in both A1 and A2; the panels differ only in the manner in which the pseudocolor was mapped to the flux density scale. The red arrows indicate the primary ROI, the green arrows indicate the metastasis ROI, and blue arrows indicate metastatic foci in both panels. (B1 and B2) Example of correspondence between a large metastatic focus on a bioluminescence image and tumor growth observed at necropsy (orange arrows) in an animal implanted orthotopically with 2×10^5 AsPC-1 cells and imaged 35 days post implant. The red arrow indicates the primary ROI and the green arrow indicates the metastasis ROI.

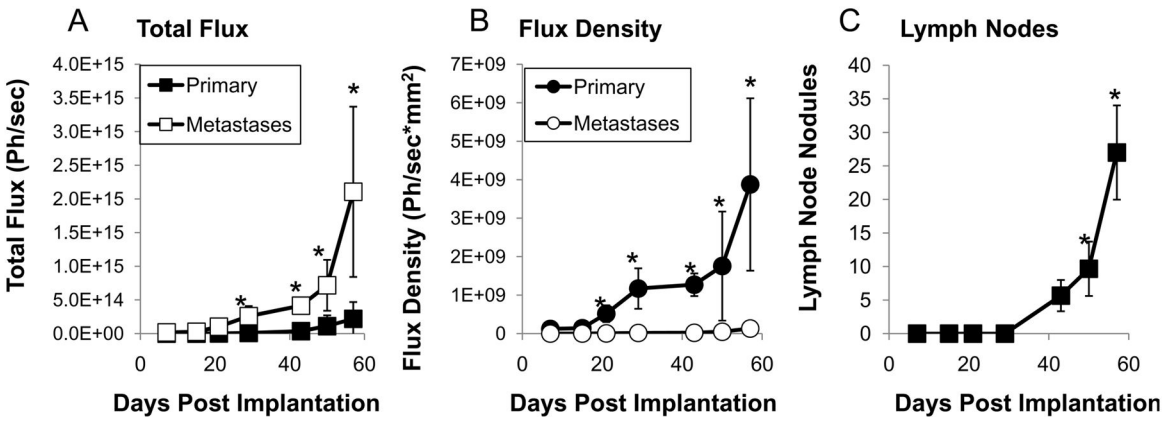

Figure 2.

Growth of primary tumor and abdominal metastatic burden in mice orthotopically implanted with Panc-1 cells. Data are expressed either as the total flux in photons/sec in each ROI (A), the average flux density in photons/sec*mm^2 (B), or as the average number of lymph node nodules (C). *$p < 0.05$ vs. baseline, Holm-Sidak post-hoc test.

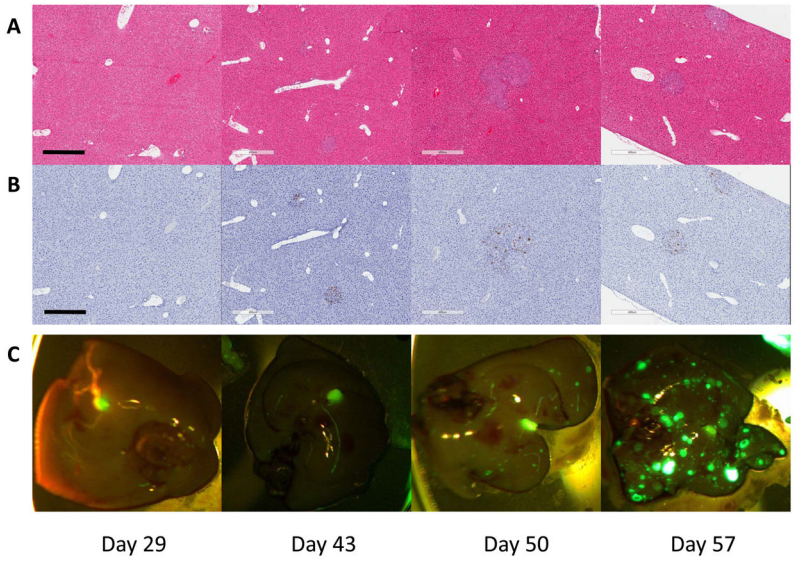

Figure 3.

Representative histological and green fluorescent protein images of liver metastases from mice orthotopically implanted with Panc-1 cells. (A) Hematoxylin and eosin stained liver sections (magnification 5X). (B) Ki67 stained liver sections (magnification 5X). (C) Green fluorescent protein images of liver *ex vivo*. Images in each column are from the same animal. Scale bar in A, B = 400 μm.

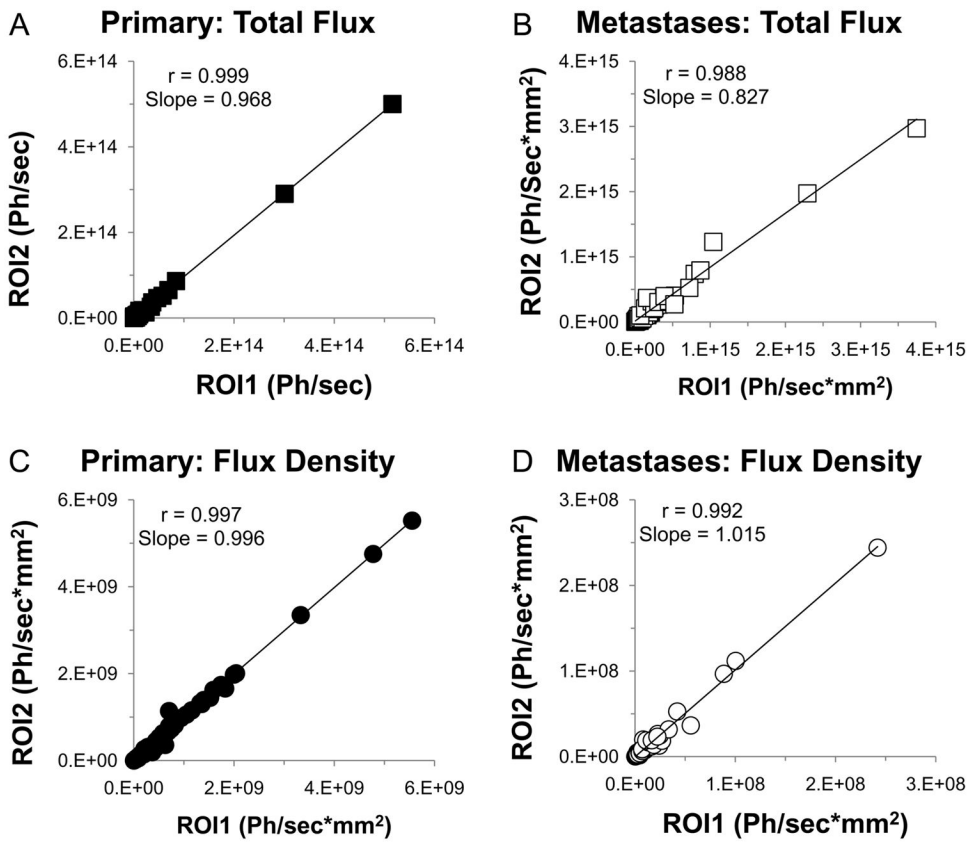

Figure 4.

Interobserver correlations for the primary (A,C) and metastases (B,D) ROIs expressed as either total flux in photons/sec (A,B) or average flux density in photons/sec*mm^2 (C,D) from mice orthotopically implanted with Panc-1 cells. Data from all animals for all of the 8 weekly imaging sessions were included in the correlations.

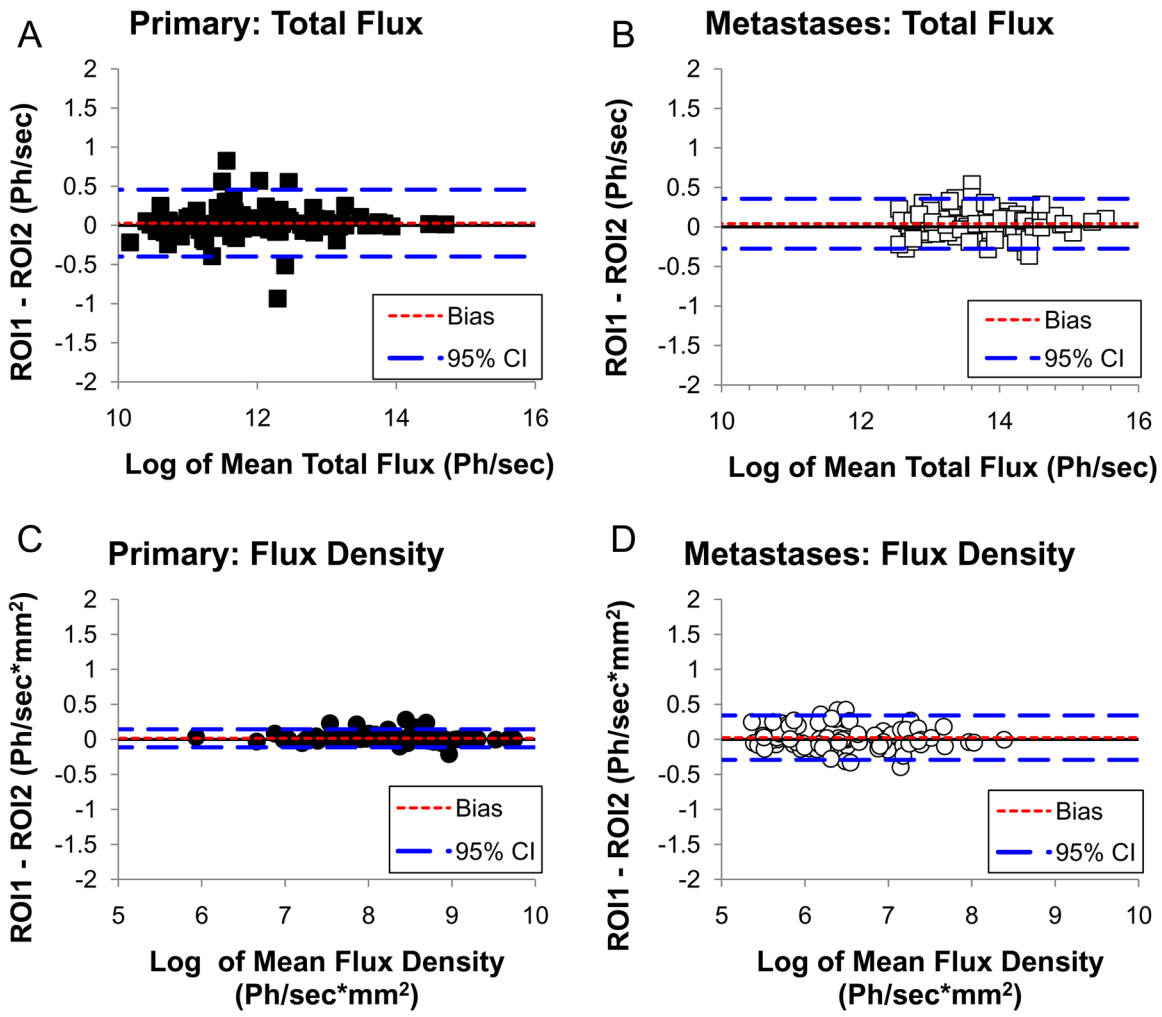

Figure 5.

Limits of agreement (Bland-Altman) plots on logarithmically transformed data for the primary (left panels) and metastasis (right panels) ROIs expressed as either total flux in photons/sec (A,B) or average flux density in photons/sec*mm2 (C,D) from mice orthotopically implanted with Panc-1 cells. Data from all animals for all of the 8 weekly imaging sessions were included in the plots. Each point represents the difference between observer 1 (ROI1) and observer 2 (ROI2) for an individual animal. The abscissa is the mean of the two observations. The bias (mean difference between the two observers across all animals) is indicated by the dashed red line and the 95% confidence limits are indicated by the dashed blue lines.

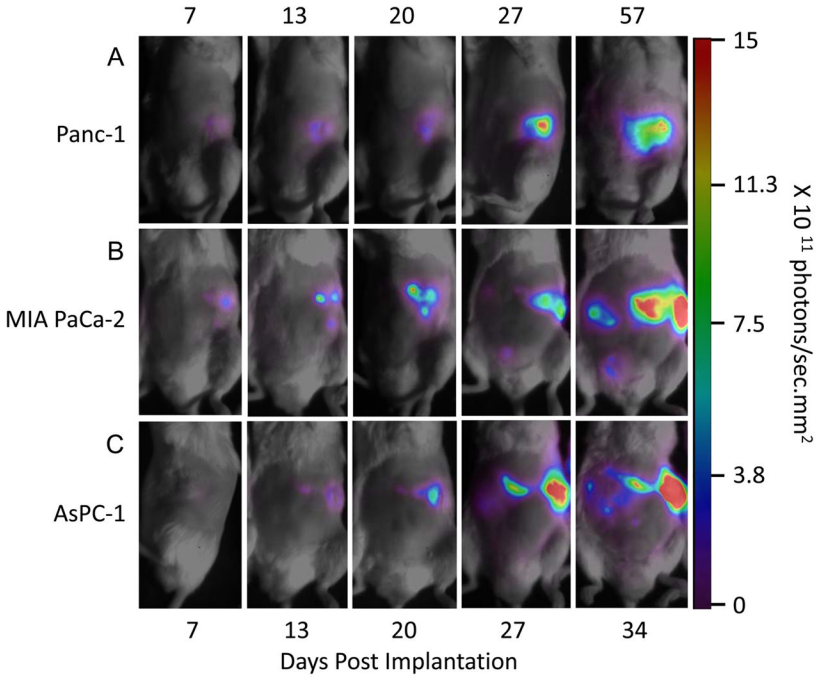

Figure 6.

Representative bioluminescence images of animals implanted orthotopically with either 2×10^6 Panc-1 (A), 2×10^5 MIA Paca-2 (B) or 2×10^5 AsPC-1 (C) pancreatic tumor cells. Numbers above the panels are the days post implant for the Panc-1 tumors and numbers below the panels are the days post implant for the MIA PaCa-2 and AsPC-1 tumors.

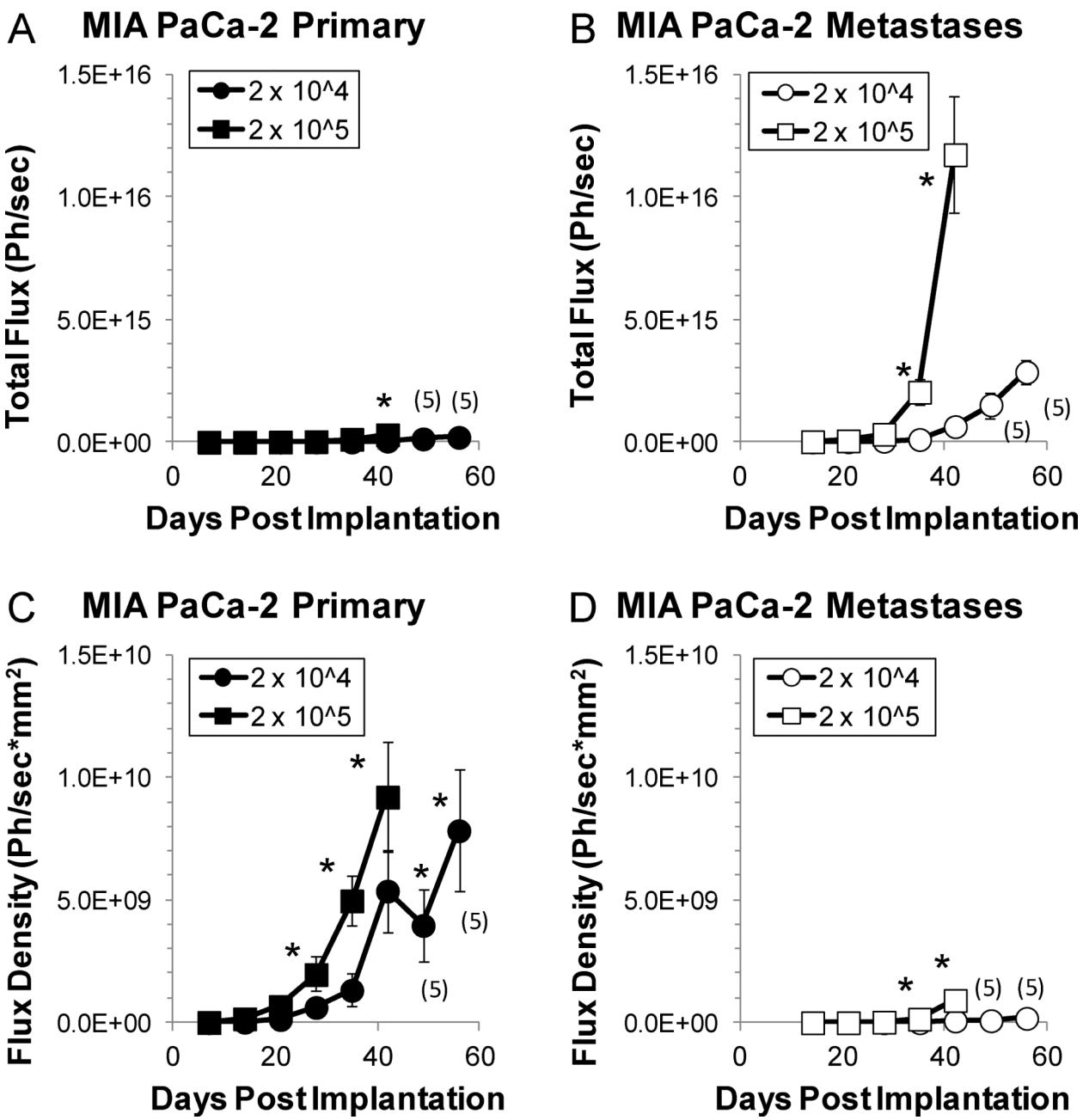

Figure 7.

Growth of primary tumor and abdominal metastases in mice orthotopically implanted with MIA PaCa-2 cells. Data are expressed either as the total flux in photons/sec in each ROI (A, B) or as the average flux density in photons/sec*mm^2 (C, D). *$p < 0.05$ vs. baseline, Holm-Sidak post-hoc test. N = 6/group unless otherwise indicated in parentheses.

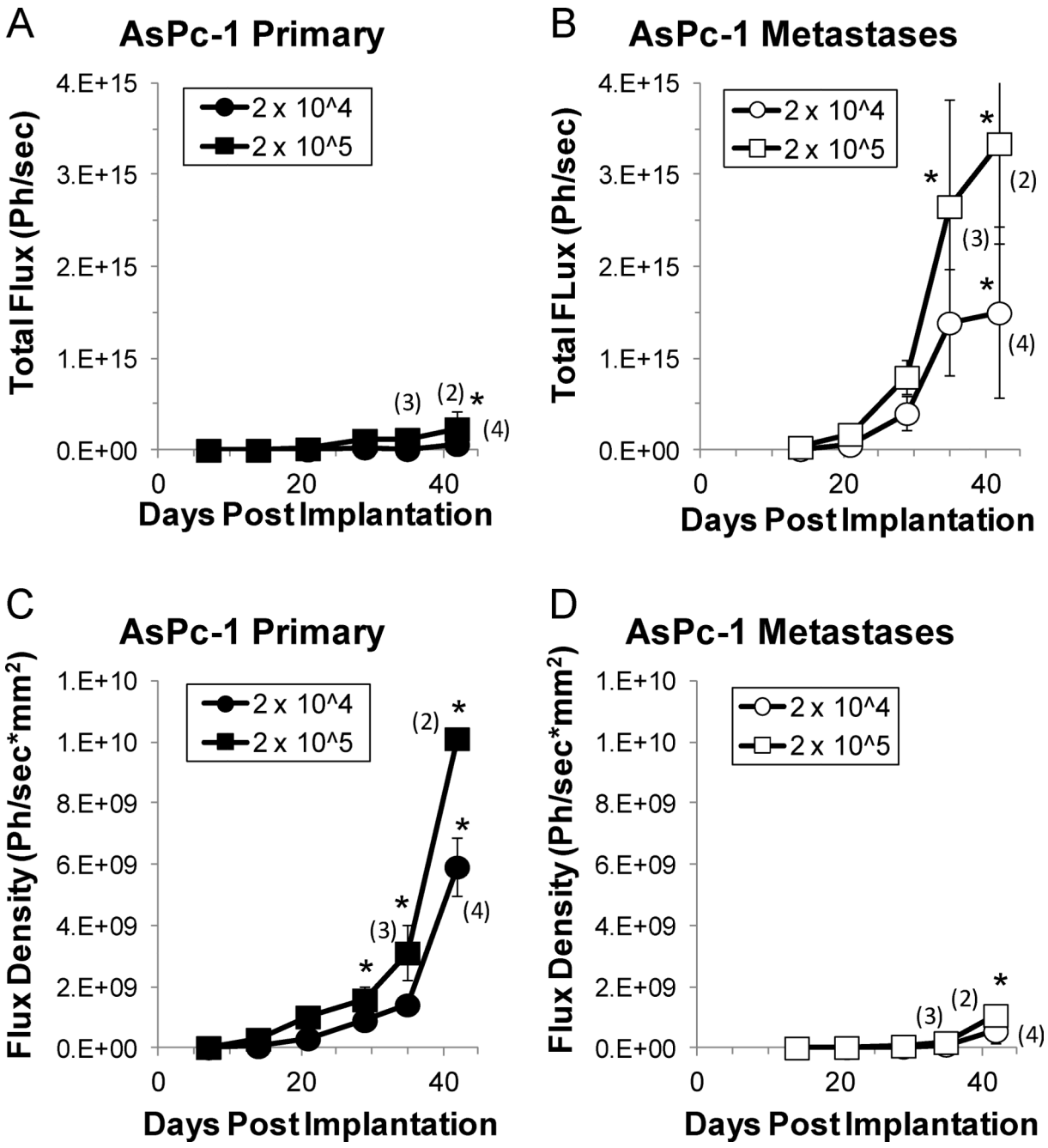

Figure 8.

Growth of primary and abdominal metastases in mice orthotopically implanted with AsPC-1 cells. Data are expressed either as the total flux in photons/sec (A, B) or as the average flux density in photons/sec*mm^2 (C, D). *$p < 0.05$ vs. baseline, Holm-Sidak post-hoc test. N = 5 for the 2×10^4 group and N = 6 for the 2×10^5 group unless otherwise indicated in parentheses.

Table 1

Percentage of mice surviving over time after orthotopic implantation of Panc-1, MIA PaCa-2 or AsPC-1 pancreatic cancer cells

NSG mice were implanted orthotopically with the cell line and number of cells indicated and bioluminescence imaging was conducted on the indicated day post implant.

Panc-1		Mia PaCa-2			AsPC-1		
Day Post Implant	2×10^6 % Surviving (N = 33)	Day Post Implant	2×10^4 % Surviving (N = 6)	2×10^5 % Surviving (N = 6)	Day Post Implant	2×10^4 % Surviving (N = 5)	2×10^5 % Surviving (N = 6)
7	100	7	100	100	7	100	100
15	100	14	100	100	14	100	100
21	100	21	100	100	21	100	100
29	100	28	100	100	29	100	100
36	100	35	100	100	35	100	50
43	100	42	100	100	42	80	33
50	100	49	83	17			
57	100	56	83	0			